48th AIAA Aerospace Sciences Meeting Including the New Horizons Forum and Aerospace Exposition
4 - 7 January 2010, Orlando, Florida

AIAA 2010-1041

Influence of Plasma Actuations on Forebody Side Forces and Wakes

Zijie Zhao *, Chao Gao†
Northwestern Polytechnical University, Xi'an 710072, China
Feng Liu‡, and Shijun Luo§
University of California, Irvine, CA 92697-3975

The variation of the asymmetric force and vortex wake on a 20° circular-cone forebody with angle of attack from 35° to 70° at zero sideslip are investigated. A pair of plasma actuators is designed and placed near the apex of the forebody. The pressure distributions over the forebody are measured in a low-turbulence $3.0\ m \times 1.6\ m$ low-speed open-circuit wind tunnel at freestream velocity $5\ m/s$ and Reynolds number of $50,000$ based on the cone base diameter. The pressure data are used to calculate the side force distribution along the forebody axis and to infer the salient features of the separated flow over the forebody under three modes of controls: plasma-off, plasma port-on and plasma starboard-on. Effects of the plasma actuations on vortex wake and side force over the cone forebody at angle of attack upto 70° are identified.

Nomenclature

C_n	=	yawing moment coefficient about cone base, yawing moment$/q_\infty SD$
C_p	=	pressure coefficient
C_Y	=	overall side-force coefficient, overall side force$/q_\infty S$
C_{Yd}	=	ensemble-averaged local side-force coefficient, local side force$/q_\infty d$
D	=	base diameter of circular cone forebody
d	=	local diameter of circular cone forebody
F	=	frequency of a.c. voltage source
L	=	length of circular cone forebody
q_∞	=	free-stream dynamic pressure
Re	=	free-stream Reynolds number based on D
U_∞	=	free-stream velocity
V_{p-p}	=	peak-to-peak voltage of a.c. voltage source
w	=	input power of a.c. voltage source
x	=	body-axis coordinate measured from apex to base
α	=	angle of attack
θ	=	meridian angle measured from windward generator, positive when clockwise

I. Introduction

Proportional lateral control on slender forebodies at high angles of attack is highly needed in aerodynamic design of air vehicles. The fact that the separation vortices over pointed forebodies generate large airloads

*Graduate Student, Department of Fluid Mechanics
†Professor and Associate Director, Aerodynamic Design and Research National Laboratory.
‡Professor, Department of Mechanical and Aerospace Engineering. Associate Fellow AIAA.
§Researcher, Department of Mechanical and Aerospace Engineering.

and are very sensitive to small perturbations near the body apex offers an exceptional opportunity for manipulating them with little energy input to achieve active lateral control of the verhicle in place of conventional control surfaces. It has been found experimentally that unsteady dynamic control techniques are needed to achieve this goal.[1–3] Recently, Liu et al.[4] reported wind-tunnel experiments that demonstrate nearly linear proportional control of lateral forces and moments over a slender conical forebody at high angles of attack by employing a novel design and placement of a pair of single dielectric barrier discharge (SDBD) plasma actuators near the cone apex combined with a duty cycle technique.

The flow control in Ref. 4 was restricted to the angle of attack between 35° and 50°. The control at angle of attack greater than 50° is prevented by the sign change of the asymmetric forces on the circular-cone forebody at zero side slip. It is well known that the sign changes of side force are caused by the occurrences of additional vortex separated alternately from the port and starboard side of the body to the initial vortex pair originated from the body apex.[5–7] How the plasma actuations affect the asymmetric forces and vortex flow on the circular-cone forebody[4] at high angles of attack upto 70° is investigated in the present paper.

Pressure measurements have been used to study vortex flowfield over bodies. Hall[8] found the location of boundary layer searation observed by Keener's oil flow[9] coincides well with the end of the pressure recovery in Lamont's pressure data[6] for 3.5 ogive nose tested under nearly same conditions. The primary flow features can be inferred from pressure data with orifices every 10° around the circumference of the body. Fiddes[10] annotated some salient features of separated flow about a cone at a large incidence from the experimental pressure distributions: the attachment point, separation points and a suction peak associated with a vortex core lying near the surface.

In this work, the measured pressure distribution over the circular-cone forebody[4] under plasma-off, plasma port-on and plasma starboard-on are used to infer the salient features of the separated flow, explain the variation of asymmetric forces on the conical forebody with angle of attack from 35° to 70°, and identify the effects of the plasma actuations. In the following sections, the experimental setup is described. The experinental results are presented and discussed. Finally conclusions are drawn.

II. Experimental Setup

The model is that used in Ref. 4. The model consists two separate pieces. The frontal portion of the cone is made of plastic and has a length of 150 mm. The rest of the model is made of metal. The total length of the cone is 463.8 mm with a base diameter of 163.6 mm. 252 time-averaged pressure tappings, Models 9816 and 8400 by the PSI Company, are arranged in rings of 36, every 10° around the circumference of the cone, at Stations 1 to 7 as shown in Fig. 1. Models 9816 and 8400 are read at frequency of 64 Hz and 127 Hz, respectively. The computer system was set up to output 1 and 5 s averages. A comparison of the measurements reveals that there are no differences in the 1 and 5 s average pressures in our experiments. We will present the 5 s average data next.

Two long strips of SDBD plasma-actuators are installed symmetrically on the plastic frontal cone near the apex as shown in Fig. 2(a). The plasma actuator consists of two asymmetric copper electrodes each of 0.03 mm thickness. A thin Kapton dielectric film wraps around the cone surface and separates the encapsulated electrode from the exposed electrode as shown in Fig. 2(b). The right edge of the exposed electrode shown in Fig. 2(b) is aligned with the cone at the azimuth angle $\theta = \pm 120°$, where θ is measured from the windward meridian of the cone and positive is clockwise when looking upstream (Fig. 2(a)). The length of the electrodes is 20 mm along the cone meridian with the leading edge located at 9 mm from the cone apex. The width of the exposed and encapsulated electrode is 1 mm and 2 mm, respectively. The two electrodes are separated by a gap of 1.5 mm, where the plasma is created and emits a blue glow in darkness. The plasma-actuator arrangement is intended to affect the boundary-layer separation positions on the cone surface. Care is taken in manufacturing and mounting of the frontal cone to the rear portion of the model to make sure they are well aligned. The actuators are hand-made and attached directly to the cone surface with no allowance.

Three modes of operations of the actuators are defined. The plasma-off mode corresponds to the case when neither of the two actuators is activated. The plasma port-on mode refers to the conditions when the port-side actuator is activated while the starboard-side actuator is kept off during the test. The plasma starboard-on mode refers to the conditions when the starboard-side actuator is activated while the portside actuator is kept off during the test. Each of the two actuators on the cone model is separately driven by

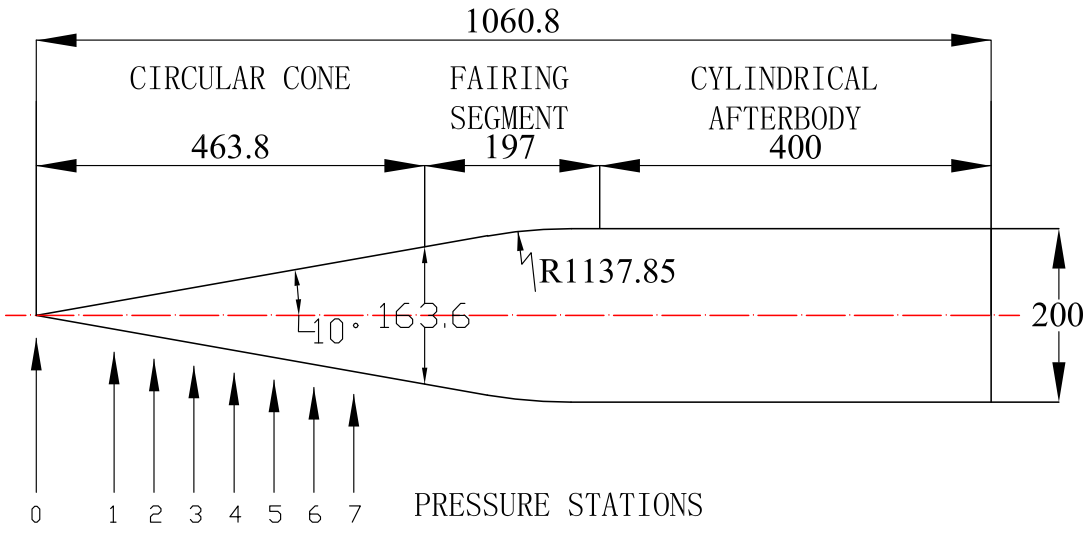

0-1	0-2	0-3	0-4	0-5	0-6	0-7
166.8	201.9	236.9	272.0	307.1	342.1	377.2

DIMENSIONS IN mm

Figure 1. The model

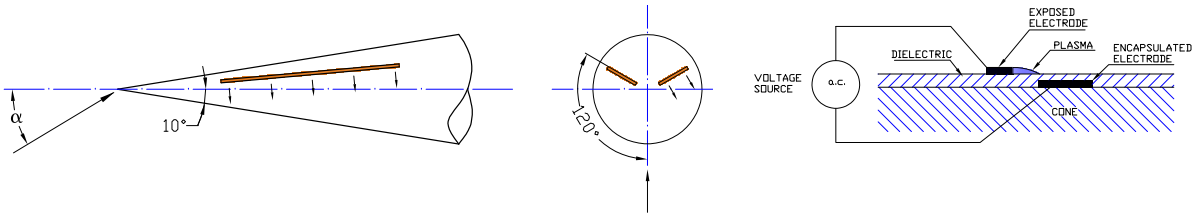

(a) arrangement (b) SDBD

Figure 2. Sketches of the plasma actuators.

an a.c. voltage source (model CTP-2000K by Nanjing Suman Co.). The waveform of the a.c. source is sine wave. The peak-to-peak voltage and frequency are set at $V_{p-p} \approx 14\ kV$ and $F \approx 8.9\ kHz$, respectively. The input power for the plasma on, $w = \approx 19.3\ W$.

The tests are conducted in a low-turbulence $3.0\ m \times 1.6\ m$ low-speed open-circuit wind tunnel at Northwestern Polytechnical University as shown in Fig. 3. The model is rigidly mounted on a support from the port side of the model aft-cylinder. The support is fixed onto the turning plate of angle of attack inbedded in the bottom wall of the wind-tunnel test-section. The model support is not symmetric with respect to the incidence plane of the model and, thus, would have an asymmetric interference on the flow around the cone forebody. The angles of attack $\alpha = 35^\circ - 70^\circ$. The free-stream velocity $U_\infty = 5\ m/s$. The Reynolds number based on the cone base diameter is $50,000$. Lateral force and moment are calculated from the measured pressures. The local side-force coefficient C_{Yd} and the overall side-force coefficient C_Y are normalized with the local and the base diameter of the cone, respectively, and are positive when pointing to the starboard side of the cone. The yawing moment coefficient C_n is normalized with the base diameter of the cone and is positive when yawing to the starboard side of the cone.carefully cleaned prior to each run of the windtunnel.

Figure 3. Model in the wind tunnel, leeward view

III. Base Plasma-Off Flow at Zero Angle of Attack

In order to check the accurary of the model setup in the wind tunnel, a test is run at zero angle of attack and with plasma off. Fig. 4 presents the time-averaged pressure distributions over the circumference of Stations $1 - 7$ at $\alpha = 0^\circ$. Aside from some slight irregularities, the measured pressure distributions indicate essentially an axisymmetric flow around the cone.

IV. Overall Side Force and Yawing Moment

Figure 5 presents the overall side force coefficient C_Y and yawing moment coefficient C_n versus angle of attack α for plasma-off, port-on and starboard-on in the range of $\alpha = 35^\circ - 70^\circ$. For plasma-off, C_Y is positive at $\alpha = 35^\circ$, increases to a maximum which is positive at $\alpha = 45^\circ$, then decreases to a minimum which is negative at $\alpha = 60^\circ$ and finally increases to a maximum which is negative at $\alpha = 65^\circ$. For port-on,

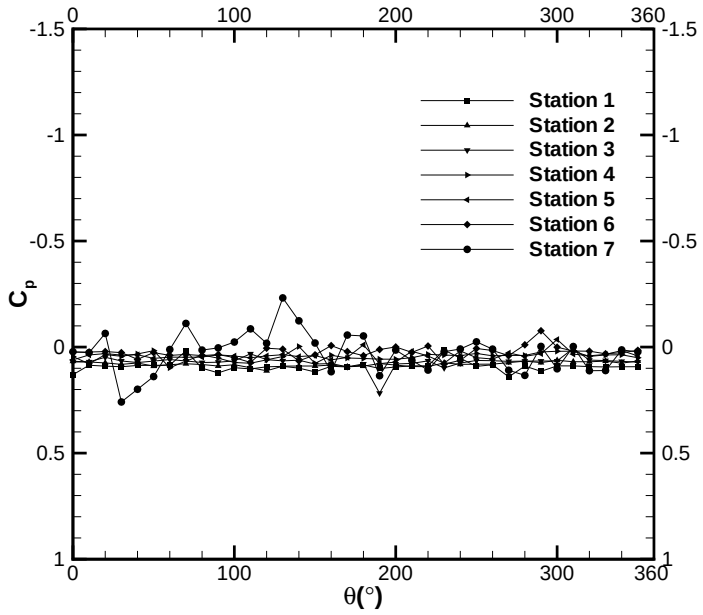

Figure 4. Time-averaged pressure distributions over circumference of various stations for plasma off, $\alpha = 0°$**,** $U_\infty = 5\ m/s$**.**

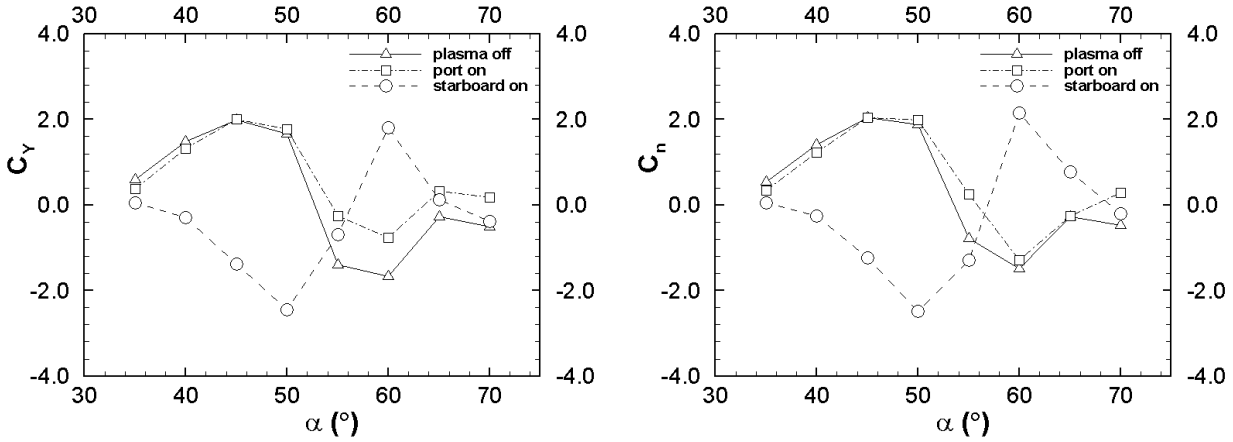

(a) side-force coefficient

(b) yawing-moment coefficient

Figure 5. Overall side force and yawing moment acting on cone forebody for plasma off and on, $U_\infty = 5\ m/s$**,** $V_{p-p} \approx 14\ kV$**,** $F \approx 8.9\ kHz$**,** $w \approx 19.3\ W$**.**

C_Y almost coincides with that for plasma-off at $\alpha = 35^\circ - 50^\circ$, decreases to a minimum which is negative at $\alpha = 60^\circ$ but greater than that for plasma-off, and then increases to a maximum which is positive at $\alpha = 65^\circ$ whereas for plasma-off C_Y remains negative. Thus, due to the the plasma actuations the magnitude of the negative minimum value of the side force at $\alpha = 60^\circ$ is decreased, and the side force recovers positive at $\alpha = 65^\circ - 70^\circ$.

The overall side forces for starboard-on and the port-on are opposite in sign but not exactly equal in magnitude at a given angle of attack. Among other factors, the imperfections of the model, particularly those due to installation of the plasma actuators mentioned earlier, are believed to have prevented the results from following the presumed exact bistable behavior.

The variation of the yawing moment with α for the three modes are similar to that of the overall side force. Similar characteristic results were reported in the literature. Hanff et al.[2] by means of alternating blowing from two forward facing nozzles located near the forebody apex, obtained side forces which are opposite and almost equal in magnitude between $\alpha = 30^\circ - 55^\circ$, and cross each other around $\alpha = 60^\circ$ in a wind tunnel experiment. From the force measurements of Zilliac et al.,[7] the overall side force on an ogive-cylindric body with no flow control, increases from zero to a positive large value as α increases from 20° to 42°, changes to negative value between $\alpha = 44^\circ$ and 53°, and approaches zero as $\alpha > 65^\circ$ at zero roll angle.

V. Local Side Force, Pressure Distribution and Flow Pattern

To understand the characteristics of the overall side force and yawing moment shown in Figure 5, the local or cross-sectional side force distributions along the body axis and the wake flow patterns over the forebody are studied. The local side force coefficient C_{Yd} at seven pressure-measurement stations and angle of attack from 35° to 70° with an increment of 5° are first listed. The two stations whose local side forces are opposite in sign are the locations where the vortex lying closer to the body surface changes from one side to the opposite side. The configuration of asymmetric vortex cores in the cross-flow plane of the stations are inferred from the corresponding pressure distribution. Thus, the overall vortex flow pattern over the circular-cone forebody is predicted.

It is known that the asymmetric vortex pair is initially originated at the sharp apex of slender body at high angles of attack and zero sideslip.[7] As the angle of attack is increased, the vortex pair is lifted away from the body surface. The vortex which lies further away on a side of the body is detached from the body surface as angle of attack is further increased. In the meantime, a new (additional) vortex is separated from the body surface underneath the run-away vortex and lies closer to the body surface than the vortex on the other side of the body. As the angle of attack is further increased, additional vortices will appear alternately on port and starboard side of the body.[5]

A. Plasma-Off

Table 1. Local side force distribution along body axis for plasma-off, $\alpha = 35^\circ - 70^\circ$, $U_\infty = 5\ m/s$.

	Pressure measurement positions, x/L						
α	0.360	0.435	0.510	0.586	0.662	0.738	0.813
35°	0.254	0.288	0.126	0.334	0.342	0.346	0.398
40°	0.717	0.778	0.660	0.830	0.860	0.851	0.896
45°	1.279	1.258	1.004	1.177	1.114	1.024	1.042
50°	1.440	1.268	0.962	0.979	0.895	0.763	0.706
55°	0.676	0.107	−0.563	−0.854	−1.113	−1.326	−1.297
60°	−0.156	−0.981	−1.132	−1.416	−1.369	−1.134	−0.900
65°	−0.062	−0.240	−0.157	−0.361	−0.265	−0.188	−0.087
70°	0.052	−0.537	−0.442	−0.608	−0.492	−0.353	−0.193

Tabe 1 presents the local side force coefficient C_{Yd} at the seven pressure-measurement stations for plasma-off at $\alpha = 35^\circ - 70^\circ$, $U_\infty = 5\ m/s$. At angle of attack $\alpha = 35^\circ - 50^\circ$, the local side force remains positive over all pressure-measurement stations. The local side force experiences the first sign change at $\alpha = 55^\circ$, from

positive at Station 2 to negative at Station 3. As the angle of attack is further increased to 60°, the local side force becomes negative over the seven Stations. However, the local side force sign-change which occurs at $\alpha = 55°$ would not disappear over the forebody at $\alpha = 60°$. The sign-change location of the local side force is the occurrence position of a new (additional) vortex. Once that a new vortex occurs, it would not disappear as the angle of attack increases. In fact, the new vortex occurrence position or the sign-change location moves forward as the angle of attack increases. In this case, it moves to the front of Station 1, which can not be detected by the present pressure measurements. When $\alpha = 70°$ the local side force is positive at Station 1. Since at $\alpha = 65°$ the local side force is negative over all pressure Stations, the positive sign of the local side force at Station 1 at $\alpha = 70°$ indicates that a sign change from negative to positive occurs in front of Station 1 at $\alpha = 70°$. Another sign change at $\alpha = 70°$ is from positive at station 1 to negative at Station 2. Therefore, at $\alpha = 70°$ the local side force changes sign three times along the cone axis. Starting from the cone apex towards downstream, the first sign-change is from positive to negative, the second is from negative to positive and the third is from positive to negative. Both first and second sign-changes occur in front of Station 1.

At $\alpha = 55°$ the pressure distributions and the inferred vortex cores at Stations 2 and 3 are plotted in Fig. 6, where the local side force coefficient C_{Yd} are inserted and S_p and S_s denote the boundary-layer separation point on the port and starboard side of the cone, respectively. On each side of the pressure station there exist two suction peaks. The first suction peak is formed due to the cross-sectional circular shape of the cone. After the first suction peak, a small amount of pressure recovery takes place before boundary-layer separation occurs at the point S_p and S_s.[8] The second suction is associated with a vortex core lying near the body surface.[10] At $\alpha = 55°$, on Station 2 the boundary-layer separation points, S_p and S_s are located at $\theta = 100°$ and $-100°$, respectively, the first suction peak on starboard side is higher than that on port side and the local side force is positive. The second suction peak on the starboard side is lower than that on the port side, but the width of the former is larger. Thus, the starboard vortex core could lie closer to the cone surface than the port vortex core as shown in Fig. 6 (a). On Station 3 the boundary-layer separation points, S_p and S_s are located at $\theta = 100°$ and $-90°$, respectively. Both first and second suction peaks on port side are higher than those on starboard side, and the local side force becomes negative at Station 3, which indicates that a vortex core is newly separated from the port side of Station 3, and located closer to the cone surface than the starboard vortex core. The occurrence of the new (additional) vortex core on port side between Stations $2-3$ at $\alpha = 55°$ is due to that the distance between the port vortex core and the body surface at Station 2 is so large that the port vortex core tends to be detached from the body surface. There are two vortex cores on port side and one vortex core on starboard side in the cross-flow plane of Station 3 at $\alpha = 55°$. Therefore, the change of the overall side force on the cone forebody from positive at $\alpha = 50°$ to negative at $\alpha = 55°$ is caused by the occurrence of the additional vortex on the port side.

For plasma-off, at $\alpha = 60° - 65°$ the local side force experiences no sign change along the cone axis and no new vortex cores occur. Thus, the overall side force remains negative at the two angles of attack. Fig. 7 presents the pressure distributions and the inferred separation vortex cores at $\alpha = 70°$ on Stations 1 and 2. At Station 1, S_p and S_s are located at $\theta = 100°$ and $-100°$, respectively. The corresponding suction peaks on both sides are almost of the same height. However, the width of the second suction peak on starboard side is larger than that on port side. Accordingly, the local side force is positive at Station 1. Since the local side force is negative at $\alpha = 65°$, there must exist a sign change from negative to positive in front of Station 1, and, thus, a new separation vortex occurs on the starboard side, and lies close to the body surface (not be captured by the pressure measurements). Therefore, in the cross-flow plane of Station 1 there appear two vortex cores on each side as shown in Fig. 7 (a). At Station 2, S_p and S_s are located at $\theta = 90°$ and $-90°$, respectively. Both first and second suction peaks on port side are higher than the corresponding suction peaks on starboard side. Accordingly, the local side force is negative and a new separation vortex occurs on the port side and lies close to the body surface. There exist three vortex cores on port side and two vortex cores on starboard side in the cross-flow plane of Station 2. As C_{Yd} is positive only on a short body length in front of Station 1, C_Y remains negative at $\alpha = 70°$ for plasma-off.

Table 2. Three additional vortices over cone forebody as α increases from $35°$ to $70°$ for plasma-off, $U_\infty = 5\ m/s$.

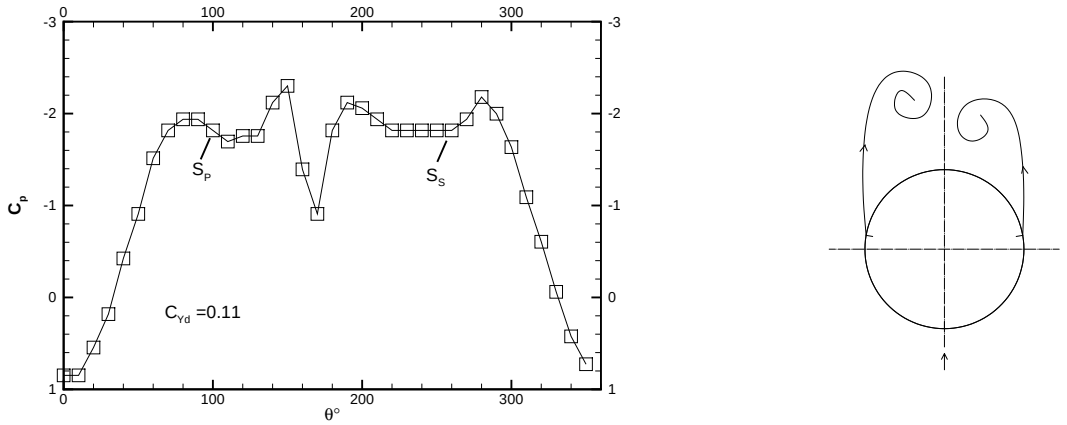

(a) Station 2

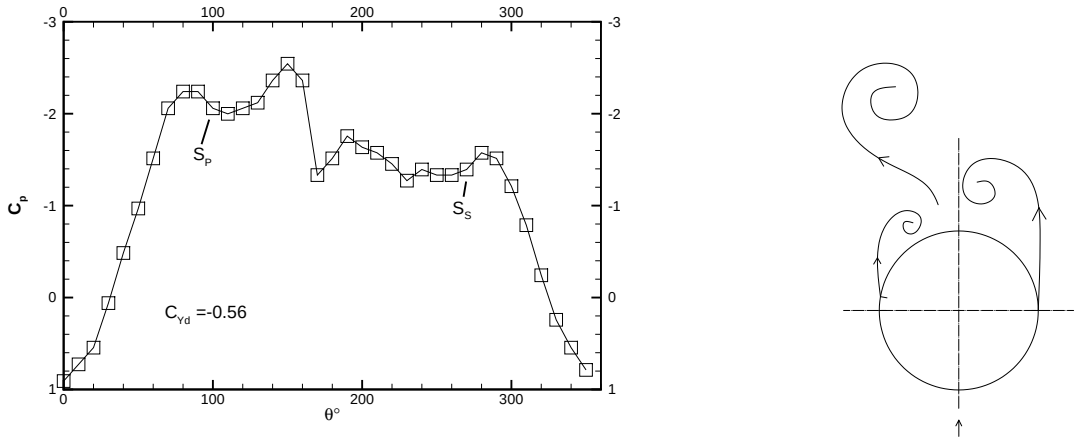

(b) Station 3

Figure 6. Separated vortex cores inferred from pressures distribution for plasma-off, $\alpha = 55°$.

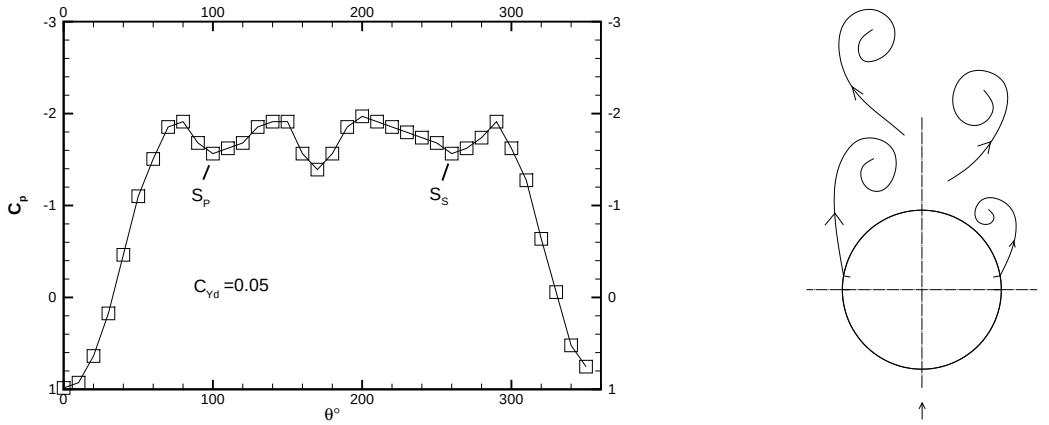

(a) Station 1

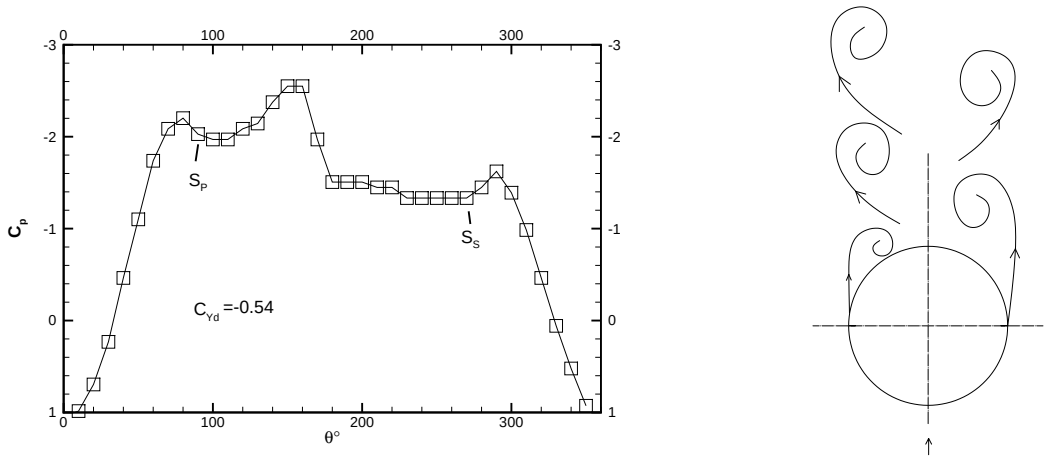

(b) Station 2

Figure 7. Separated vortex cores inferred from pressures distribution for plasma-off, $\alpha = 70°$.

Additional vortex	α°	Port/starboard side	Location between
1st	55°	port	Station 2 and 3
2nd	70°	starboard	Apex and Station 1
3rd	70°	port	Station 1 and 2

The occurrence of three additional vortex cores for plasma-off is listed in Table 2. Fig. 8 sketches the overall vortex flow pattern over the circular-cone forebody for plasma-off at $\alpha = 45^\circ$ to 70°, where the shear layer which extends from the separation point to the remote rolling-up vortex core is not shown for clarity.[5] The flow patterns at $\alpha = 35^\circ$ and 40° are the same as that of $\alpha = 45^\circ$ (not shown here for brevity). For plasma-off, the first additional vortex occurs on port side of the cone at $\alpha = 55^\circ$ between Stations $2-3$, the second additional vortex occurs on starboard side at $\alpha = 70^\circ$ in front of Station 1 and the third additional vortex occurs on port side at $\alpha = 70^\circ$ between Stations $1-2$. The occurrences of the three new (additional) vortices match with the variation of the overall side force as the angle of attack is increased From 55° to 70°. The present predictions on the vortex-flow patterns are pending to be verified by other methods.

B. Plasma Port-On

Local side force distribution and flow pattern variation for plasma port-on are investigated. Tabe 3 presents the local side force coefficient C_{Yd} along the body axis for port-on when the angle of attack is increased from $\alpha = 35^\circ$ to 70° at $U_\infty = 5\ m/s$. The local side force experiences one sign change along the cone axis at each of the four angles of attack, 55°, 60°, 65° and 70°. At $\alpha = 55^\circ$ the local side force changes from positive at Stations 3 to negative at Station 4. At $\alpha = 60^\circ$ the local side force changes from negative at Stations 6 to positive at Station 7. At $\alpha = 65^\circ$ the local side force changes from negative at Stations 3 to positive at Stations 4. The sign change at $\alpha = 65^\circ$ is the same as that at $\alpha = 60^\circ$ but the sign change position moves forward. At $\alpha = 70^\circ$ the local side force changes from positive at Stations 5 to negative at Station 7. At Station 6 the magnitude of local side force is almost zero.

Table 3. Local side force distributions along body axis for port-on, $\alpha = 35^\circ - 70^\circ$, $U_\infty = 5\ m/s$.

	Pressure measurement positions, x/L						
α	0.360	0.435	0.510	0.586	0.662	0.738	0.813
35°	0.166	0.213	0.014	0.212	0.205	0.222	0.264
40°	0.584	0.636	0.547	0.753	0.753	0.772	0.810
45°	1.217	1.230	1.062	1.193	1.137	1.081	1.042
50°	1.494	1.345	1.024	1.056	0.947	0.824	0.760
55°	0.910	0.599	0.125	−0.010	−0.225	−0.481	−0.640
60°	−1.331	−1.322	−1.046	−0.737	−0.350	−0.056	0.153
65°	−1.054	−0.716	−0.078	0.107	0.372	0.552	0.722
70°	0.239	0.253	0.448	0.191	0.112	−0.003	−0.044

The pressure distributions with the inferred separation vortex cores at $\alpha = 55^\circ$, 60° and 70° are presented in Figs. 9, 10 and 11, respectively. $\alpha = 65^\circ$ is not considered here because the sign change is the same as of $\alpha = 60^\circ$.

There appear three additional vortices at $\alpha = 55^\circ, 60^\circ$ and 70° for port-on. Table 4 lists the occurrence locations of the additional vortices for port-on. Fig. 12 sketches the overall vortex flow pattern for port-on at $\alpha = 45^\circ$ to 70°.

In the present wind tunnel run, the plasma-off results almost cioncide with the port-on results at moderate high angles of attack. They differ from each other when the angle of attack is high. Their differences yield the effects of the effcts of the plasma actuations. At $\alpha = 55^\circ$ due to the plasma actuation the first additional vortex occurs at a downstream location, and the overall side force changes to a negative value of smaller magnitude. After the occurrence of the first additional vortex, due to the plasma actuations the occurrence of the new vortices is more evenly distributed over the range of the angle of attack upto 70°, and the sign of the overall side force could change back to positive while it stays negative for plasma-off.

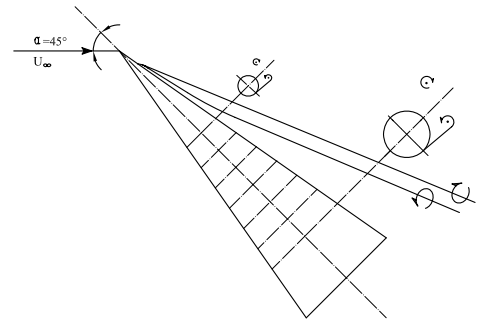

(a) $\alpha = 45°$

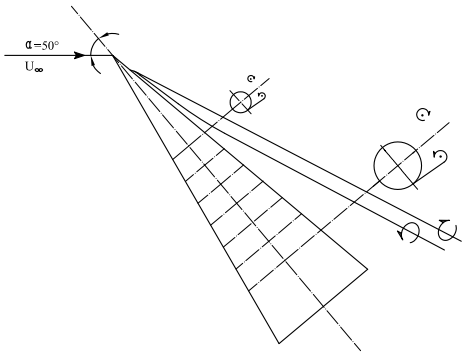

(b) $\alpha = 50°$

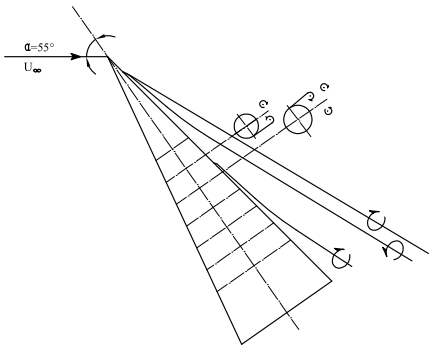

(c) $\alpha = 55°$

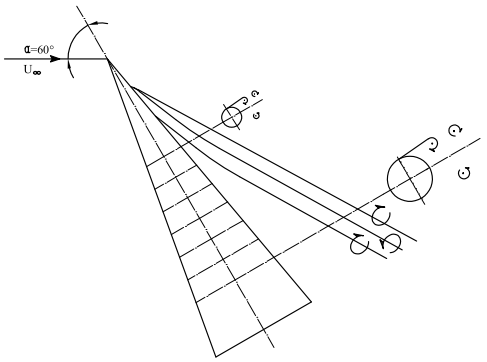

(d) $\alpha = 60°$

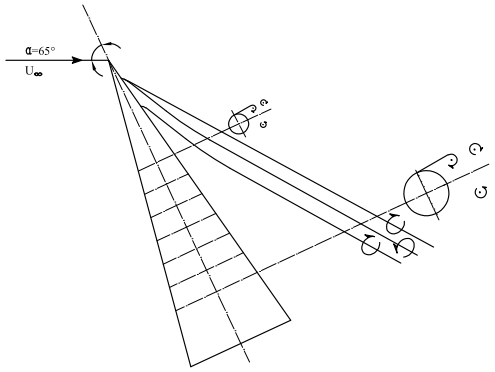

(e) $\alpha = 65°$

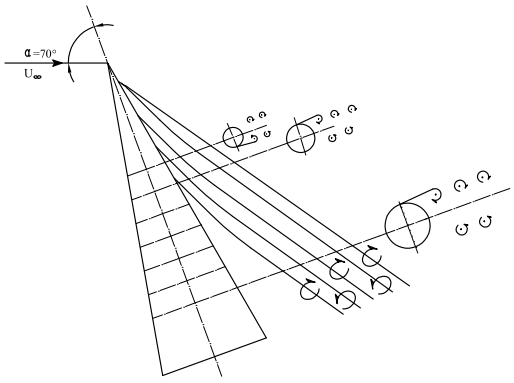

(f) $\alpha = 70°$

Figure 8. Sketch of wake from cone forebody at large incidences for plasma-off, $U_\infty = 5\ m/s$.

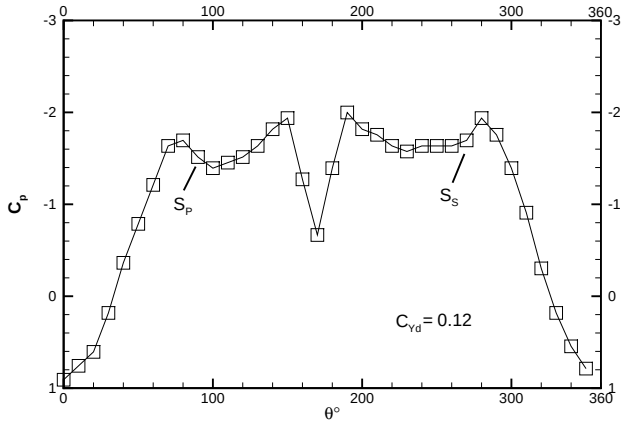

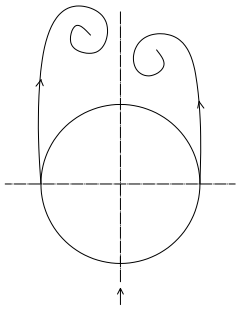

(a) Station 3

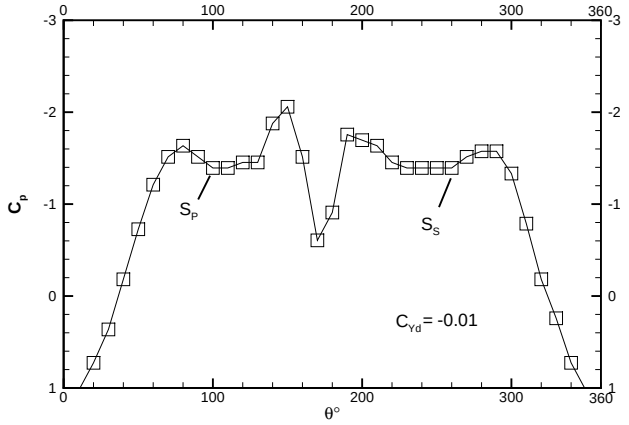

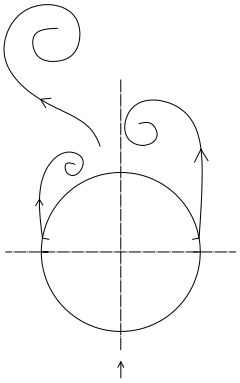

(b) Station 4

Figure 9. Separated vortex cores inferred from pressures distribution for port-on, $\alpha = 55^\circ$.

Table 4. Three additional vortices over cone forebody as α increases from 35° to 70° for port-on, $U_\infty = 5\ m/s$.

Additional vortex	α°	Port/starboard side	Location between
1st	55°	port	Station 3 and 4
2nd	60°	starboard	Station 6 and 7
3rd	70°	port	Station 5 and 7

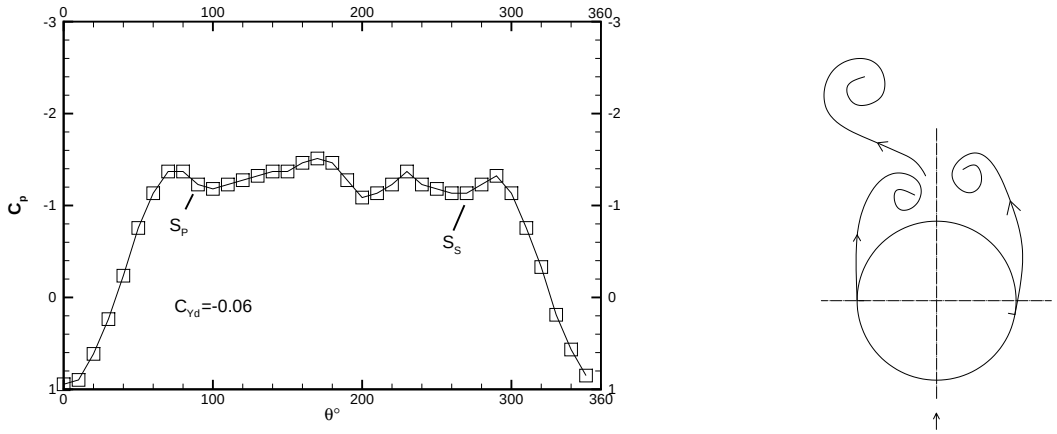

(a) Station 6

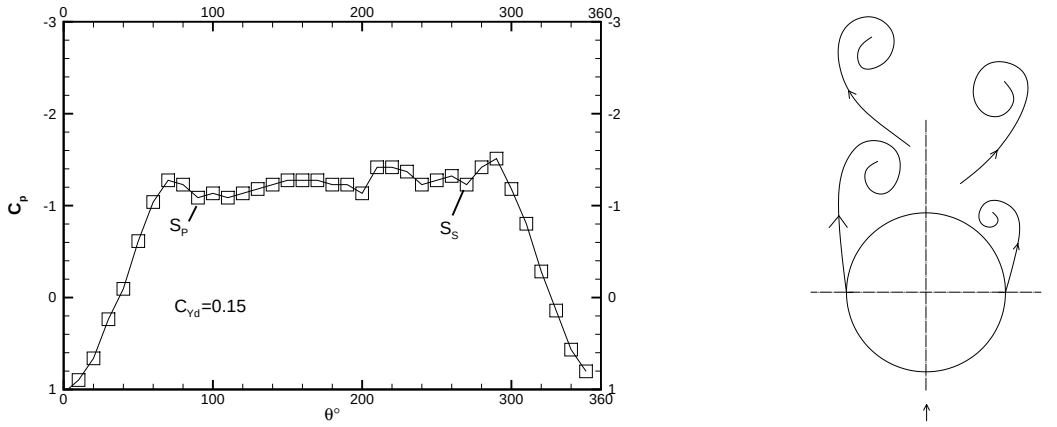

(b) Station 7

Figure 10. Separated vortex cores inferred from pressures distribution for port-on, $\alpha = 60°$.

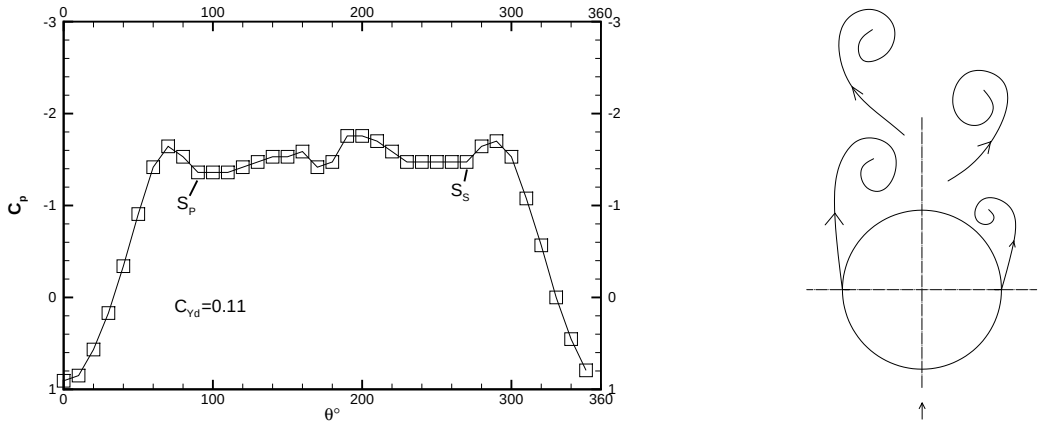

(a) Station 5

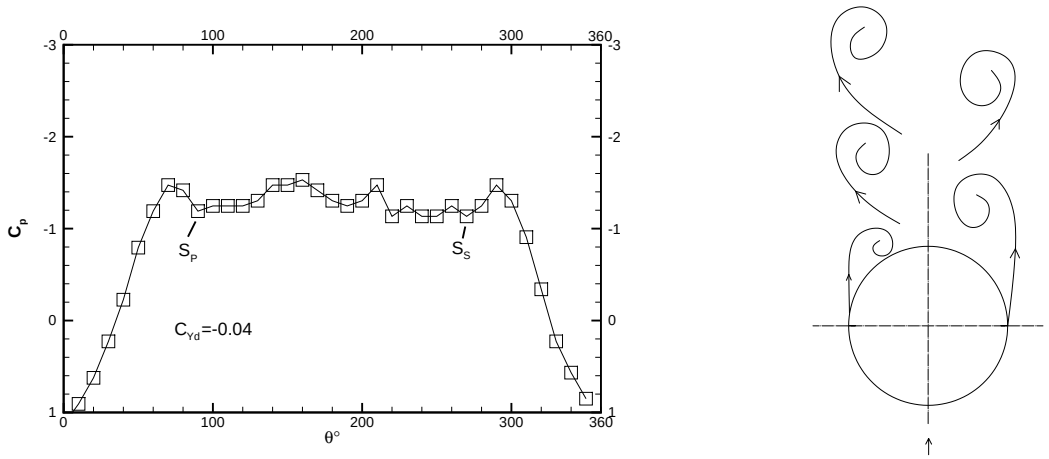

(b) Station 7

Figure 11. Separated vortex cores inferred from pressures distribution for port-on, $\alpha = 70°$.

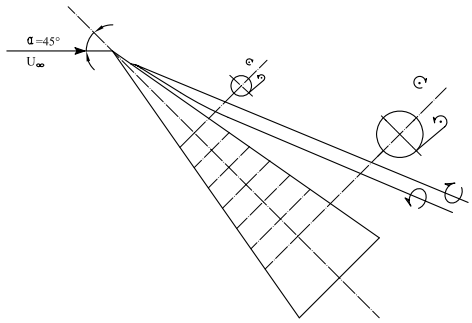

(a) $\alpha = 45°$

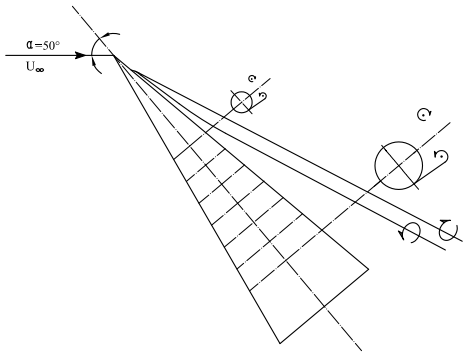

(b) $\alpha = 50°$

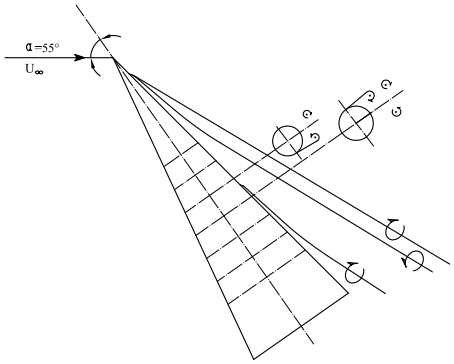

(c) $\alpha = 55°$

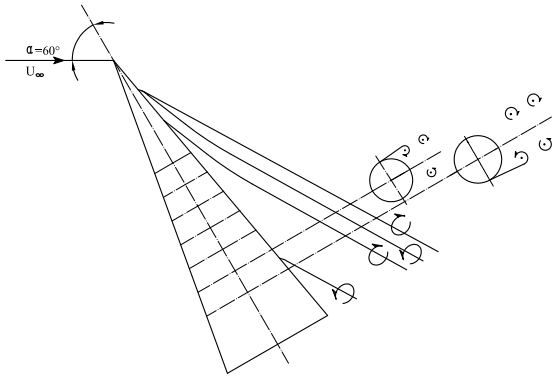

(d) $\alpha = 60°$

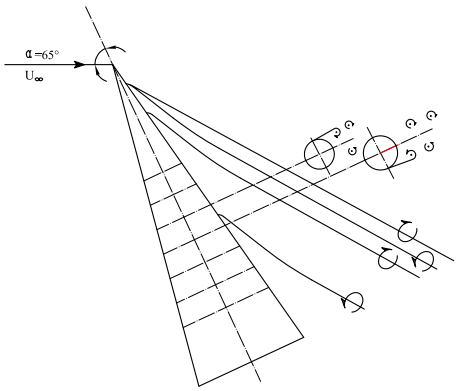

(e) $\alpha = 65°$

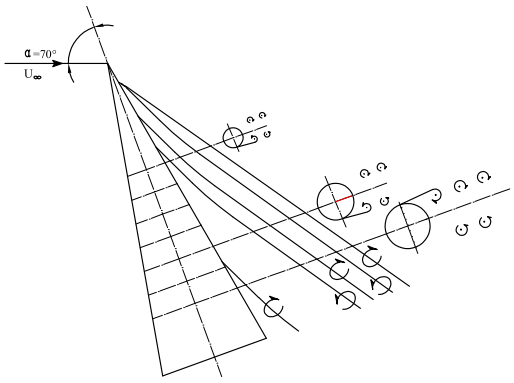

(f) $\alpha = 70°$

Figure 12. Sketch of wake from cone forebody at large incidences for port-on, $U_\infty = 5\ m/s$.

C. Plasma Starboard-On

For starboard-on, Fig. 5 shows that the overall side force is almost opposite in sign with respect to that for port-on at a given angle of attack. Table 5 presents the local side force coefficient C_{Yd} at various pressure measurement stations for starboard-on at $\alpha = 35^\circ - 70^\circ$, $U_\infty = 5\ m/s$. At $\alpha = 35^\circ$, the overall side force is nearly zero, and so are the local side forces along the cone axis. The sign-changes around Station 3 are insignificant for the present study, and not considered here. As the angle of attack is increased, the actuation of starboard plasma actuator becomes effective. At $\alpha = 40^\circ, 45^\circ$ and 50°, the local side force is negative over all the Stations $1 - 7$. At $\alpha = 55^\circ$, the local side force experiences the first sign change, from nagative at Station 6 to positive at Station 7. At $\alpha = 60^\circ$, the local side force remains positive throughout the seven Stations and no addtional vortex occurs. At $\alpha = 65^\circ$, the local side force experiences the second sign change from positive at Station 4 to negative at Station 5. At $\alpha = 70^\circ$, the local side force experiences a sign change same as that of $\alpha = 65^\circ$, but the sign-change location moves upstream to from positive at Station 1 to negative at Station 2. No additional vortex appears at $\alpha = 70^\circ$.

Table 5. Local side force distributions along body axis for starboard-on, $\alpha = 35^\circ - 70^\circ$, $U_\infty = 5\ m/s$.

	Pressure measurement positions, x/L						
α	0.360	0.435	0.510	0.586	0.662	0.738	0.813
35°	0.072	0.044	−0.176	0.036	0.021	0.015	0.047
40°	−0.062	−0.083	−0.313	−0.159	−0.176	−0.186	−0.176
45°	−0.430	−0.558	−0.829	−0.759	−0.808	−0.878	−0.880
50°	−1.355	−1.434	−1.630	−1.479	−1.403	−1.371	−1.258
55°	−1.468	−1.213	−1.160	−0.664	−0.331	−0.054	0.279
60°	1.491	1.559	1.583	1.353	1.153	0.846	0.542
65°	1.423	0.911	0.608	0.146	−0.093	−0.384	−0.554
70°	0.376	−0.089	−0.195	−0.511	−0.437	−0.410	−0.304

For starboard-on, there appear two additional vortex cores as the angle of attack is increased from 35° to 70° besides the vortex pair starts from the apex of the cone. The first additional vortex occurs at $\alpha = 55^\circ$ and the second additional vortex occurs at 65°. The pressure distributions with the inferred separation vortex cores at $\alpha = 55^\circ$ and 65° are studied in Figs. 13 and 14, respectively. Table 6 lists the occurrence of the two additional vortices. Fig. 15 sketches the overall vortex flow pattern for starboard-on at $\alpha = 45^\circ$ to 70°. In comparison with plasma-off, the first additional vortex for starboard-on occurs at a downstream location, and the starboard-on has fewer additional vortices as the angle of attack is increased from 35° to 70°.

Table 6. Two new vortices over cone forebody as α increases from 35° to 70° for starboard-on, $U_\infty = 5\ m/s$.

Additional vortex	α°	Port/starboard side	Location between
1st	55°	starboard	Station 6 and 7
2nd	65°	port	Station 4 and 5

VI. Conclusions

An experimental study of the variation of asymmetric force and vortex flowfield is performed on a 20° circular-cone-cylinder model at angles of attack 35° to 70° under three different modes of controls: plasma-off, plasma port-on and plasma starboard-on. The effects of the plasma actuations on the development of the separation vortex patterns and asymmetric forces on the forebody are identified.

1. As the angle of attack is increased, the occurrence of the first additional vortex besides the initial vortex pair originated from the sharp apex of the cone is delayed to a downstream location due to the plasma actuations.

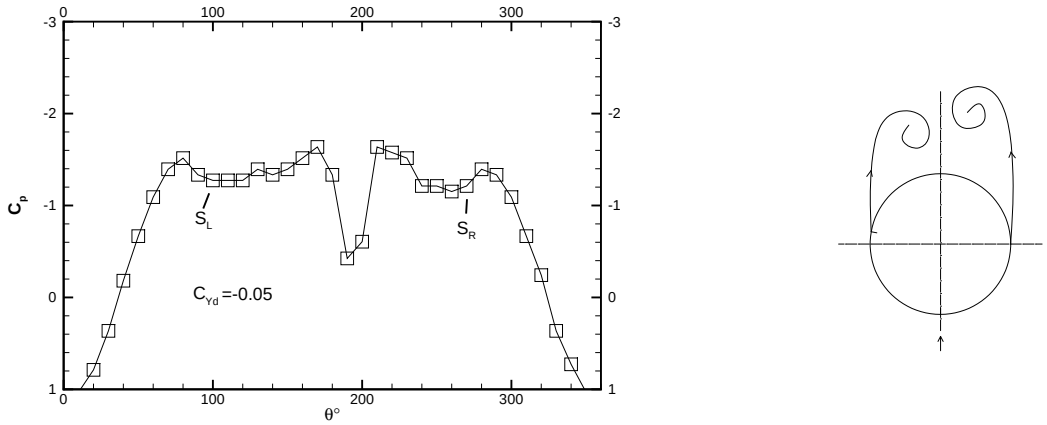

(a) Station 6

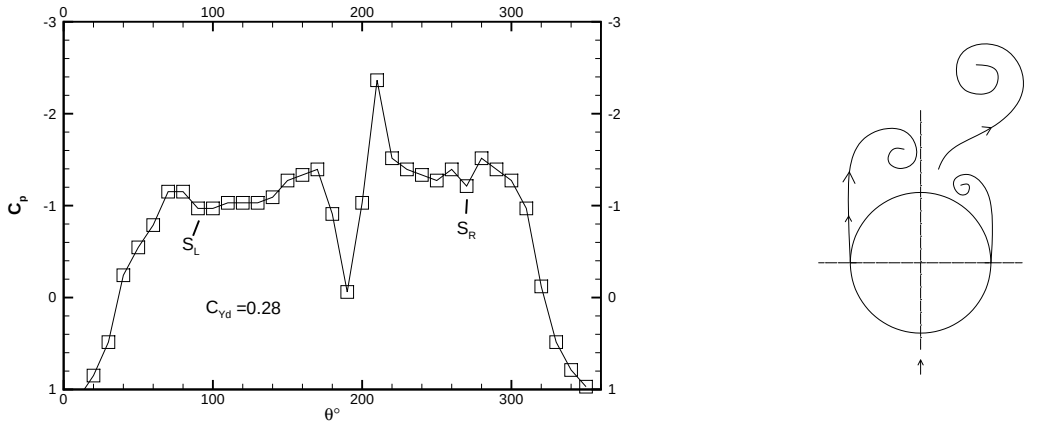

(b) Station 7

Figure 13. Separated vortex cores inferred from pressures distribution for starboard-on, $\alpha = 55°$.

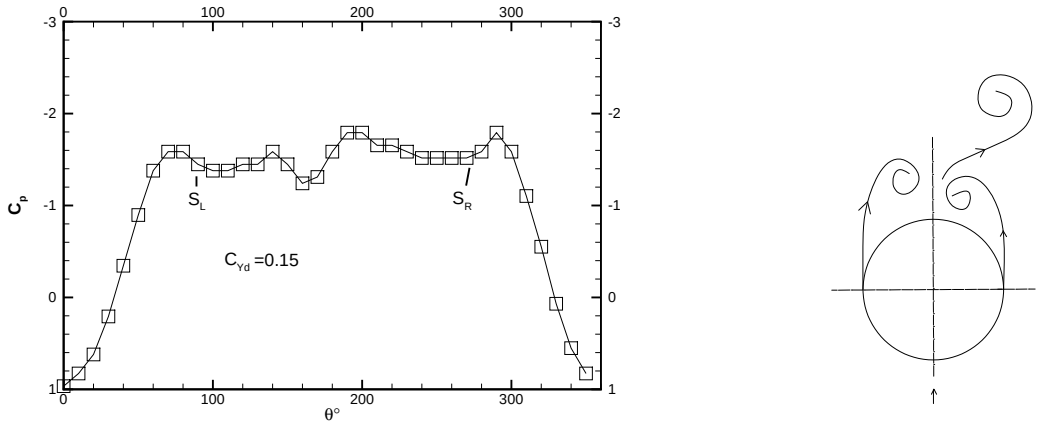

(a) Station 4

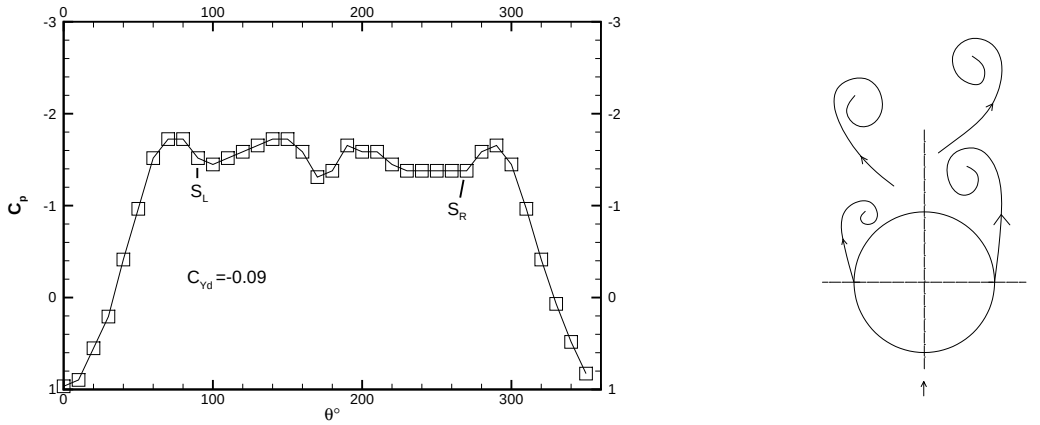

(b) Station 5

Figure 14. Separated vortex cores inferred from pressures distribution for starboard-on, $\alpha = 65°$.

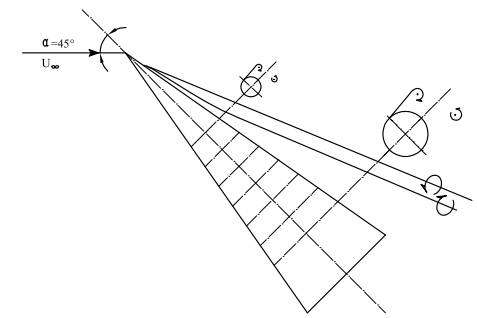

(a) $\alpha = 45°$

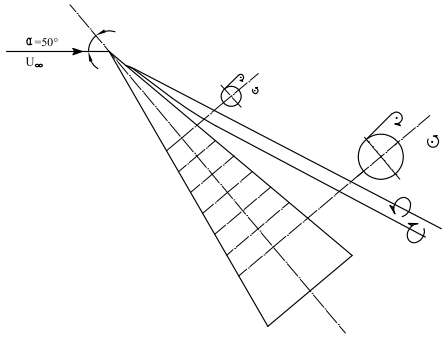

(b) $\alpha = 50°$

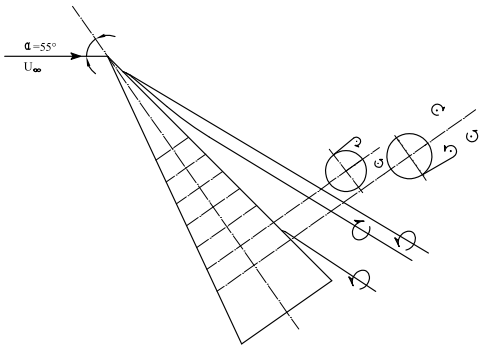

(c) $\alpha = 55°$

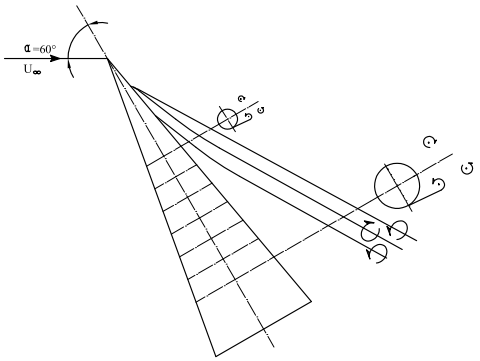

(d) $\alpha = 60°$

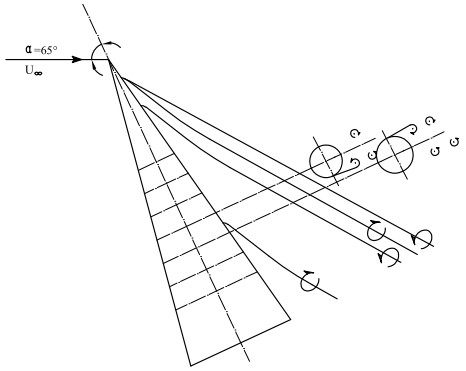

(e) $\alpha = 65°$

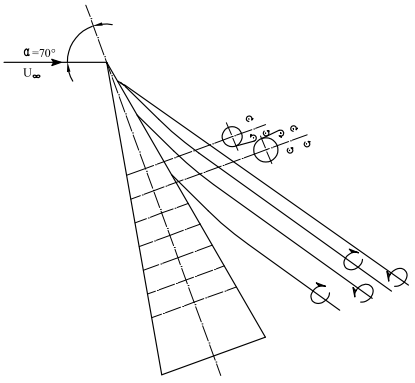

(f) $\alpha = 70°$

Figure 15. Sketch of wake from cone forebody at large incidences for starboard-on, $U_\infty = 5\ m/s$.

2. The first sign change of the asymmetric force may be delayed to a higher angle of attatck, and the corresponding magnitude change of the asymmetric force may be decreased under the plasma actuations.

3. After the occurrence of the first additional vortex, the following additional vortices occur evenly over the angle of attack range due to the plasma actuations.

4. After the first sign change of the asymmetric force the bistable behavior of the asymmetric force may appear again as angle of attack is further increased under the plasma actuations.

Verification of the vortex wake patterns inferred from the measured pressure distributions by other methods and control of the additional vortices besides the apex vortex pair to raise the angle of attack at which the overall side force first changes sign are pending to be studied.

Acknowledgments

The present work is supported by the Foundation for Fundamental Research of the Northwestern Polytechnical University, NPU-FFR-W018101 and the Specialized Research Fund for the Doctoral Program of Higher Education, SRFDP-200806990003.

References

[1]Bernhardt, J. E. and Williams, D. R., "Proportional control of asymmetric forebody vortices," *AIAA Journal*, Vol. 36, No. 11, Nov. 1998, pp. 2087–2093.

[2]Hanff, E., Lee, R., and Kind, R. J., "Investigations on a dynamic forebodey flo w control system," *Proceedings of the 18th International Congress on Instrumentation in Aerospace Simulation Facilities*, Inst. of Electrical and Electronics Ehgineers, Piscataway, NJ, 1999,pp. 28/1-28/9.

[3]Ming, X. and Gu, Y., "An innovative control technique for slender bodies at high angle of attack," AIAA Paper 2006-3688, June 2006.

[4]Liu, F., Luo, S.J.,Gao, C., Meng, X.S., Hao, J.N., Wang, J.L. and Zhao, Z.J., "Flow control over a conical forebody using duty-cycled plasma actuators," *AIAA Journal*, Vol. 46, No. 11, Nov. 2008, pp. 2969–2973.

[5]Thomson, K.D. and Morrison, D.F., "The spacing, position and strength of vortices in the wake of slender cylindrical bodies at large incidence," *Journal of Fluid Mechanics*, Vol. 50, Part 4, 1971, pp. 751–783.

[6]Lamont, P.J., "Pressure around an inclined ogive cylinder with laminar, transitional, or turbulent separation," *AIAA Journal*, Vol. 20, No. 11, Nov. 1982, pp. 1492–1499.

[7]Zilliac, G.G., Degani, D. and Tobak, M., "Asymmetric vortices on a slender body of revolution," *AIAA Journal*, Vol. 29, No. 5, May. 1991, pp. 667–675.

[8]Hall, R.M., "Influence of Reynolds number on forebody side forces for 3.5-diameter tangent-ogive bodies," AIAA-87-2274, Jun. 1987

[9]Keener, E.R., "Flow-separation patterns on symmetric forebodies" NASA TM 86016, 1986.

[10]Fiddes, S., "Separated flow about cones at incidence–theory and experiment," *Proceedings of Symposium on Studies of Vortex Dominated Flow*, NASA/LRC, 1985, pp. 285–310.

[11]Liu, F., Luo, S.J.,Gao, C., Meng, X.S., Hao, J.N., Wang, J.L. and Zhao, Z.J., "Mechanisms for conical forebody flow control using plasma actuators," AIAA Paper 2009-4284, June 2009.